

## CRUISE REPORT JC113

Robert N. Harris

Oregon State University

### **Introduction**

This report provides an operational and scientific overview of expedition JC113 on the *RRS James Cook*. Expedition JC113 is the heat flow component of the four expedition OSCAR experiment. All analysis contained in this report is preliminary as it was prepared during and at the end of scientific operations. JC113 was very successful, both operationally and scientifically. This success is directly attributable to the skill and dedication of the ship's crew and technical support staff and the outstanding facilities available on the *RRS James Cook*.

The overall goal of JC113 is to improve our understanding of how hydrothermal circulation couples the ocean and lithosphere. To achieve this goal we collected heat flow measurements on the southern flank of the Costa Rica ridge flank. The principal science objectives are to: 1) understand the thermal characteristics and heat transfer from the crust to the ocean between the Costa Rica Rift and IODP Hole 504B; 2) to provide a process-based understanding of how crustal hydrothermal circulation impacts deep ocean circulation in the Panama Basin, and 3) to understand linkages among the shallow structure of the oceanic crust, its evolution, and heat transfer.

The Costa Rica ridge flank was chosen for this work because it has been the site of numerous seismic, heat flow and ocean drilling experiments and has become an important type location for investigations of off-axis hydrothermal processes (*Anderson and Hobart, 1976; Langseth et al., 1983; Hobart et al., 1985, Refs*). The presence of Hole 504B, one of the deepest scientific boreholes drilled into the oceanic crust designed to investigate upper crustal processes adds value to considerable contextual information for understanding ridge flank hydrothermal circulation (*Anderson et al., 1982; Alt et al., 1986; Becker et al., 1989; Detrick et al., 1994*). Additionally, the Panama Basin is enclosed by the Cocos and Carnegie ridges to the west and Central and South America to the east in which the effects of geothermal heating and mixing can be isolated relative to the larger Pacific Basin.

The transport and exchange of mass, heat energy, and geochemical constituents between young lithosphere at mid-ocean ridges and the ocean is a process of fundamental importance in Earth system dynamics and constitutes a primary focus of international research programs. Over the past 3-plus decades, considerable effort has been devoted to understanding high-temperature venting at ridge axes and its links to magmatic processes, geochemical fluxes, and the crustal biosphere. Similarly hydrothermal circulation on ridge flanks has garnered much attention because huge volumes of seawater circulate through oceanic crust (*Parsons and Sclater, 1977; Mottl and Wheat, 1994; Johnson and Pruis, 2003*). Recently, ocean general circulation models predict that geothermal heating of bottom water has an appreciable influence on mixing in the abyssal ocean and potentially wider effects on global thermohaline circulation (e.g., *Hofmann and Morales Maqueda, 2009; Emile-Geay and Madec, 2009*). The interactions between crustal energy and mass discharge with the overlying ocean are not well understood.

This report describes the heat flow equipment, measurement parameters, and data collected during the cruise.

### **Multipenetration Heat Flow Probe Measurements**

All heat flow measurements were collected with using a multipenetration heat flow (MPHF) probe (**Figure 1**). The MPHF probe consists of a 3.5-m, 11-thermistor, violin-bow heat flow system maintained at Oregon State University. The design of the MPHF probe provides both the mechanical robustness to withstand repeated insertions and withdrawals from the sediment, and sensitivity needed to make highly accurate measurements. Repeated insertions of the probe allow multiple heat flow measurements to be made with a single transit through the water column increasing measurement efficiency. Temperature time series used for both the determination of the thermal gradient and thermal conductivity are logged into solid-state memory in a data logger located in the probe weight stand. Other parameters logged by the system include time, pressure (depth), water temperature, tilt, and a stable reference resistance. Acoustic telemetry during surveys relays temperature data and tilt to the surface so that instrument performance can be monitored in real time. Internal power allows stations to run 20-30 measurements when fully charged.

MPHF probe operations were run from the aft A-frame using the deep tow wire. The probe weighs 0.52 tons in water. Pull-out tension approached but did not exceed five tons. An ultra-

short baseline (USBL) transponder was attached to the wire 50 m above the weight stand for all MPHF probe operations to determine the instrument location relative to the ship. Instrument locations are estimated to be better than 25 m. Heat flow operations alternated with CTD/VMP operations.

Heat flow measurements were started by lowering the MPHF probe into the sediment at 60 m/min. Following the insertion of the probe, temperatures were interrogated every 10 seconds for 7 minutes. During this period thermistors approach thermal equilibrium with the surrounding sediment and this temperature-time series is used to compute the thermal gradient. Following this initial 7-minute period a calibrated heat pulse is generated along a heating wire within the thermistor tube. The temperature decay of this heat pulse is monitored to determine in-situ thermal conductivity. After a measurement was completed, the probe was raised to approximately 100 m above the seafloor while the ship transited at 1-2 kts to the next site.

MPHF probe heat flow data were parsed into individual penetration files and processed using SlugHeat, a Matlab based program (A. Fisher, written commun., 2005). Additional analysis will be required to finalize the heat flow values listed in this report (**Table 1**), but values are unlikely to change by more than a few percent as a result of reanalysis. No corrections have been applied for at this stage for instrument tilt (generally less than about 3°), sedimentation, or local topography.

In total six heat flow stations consisting of 85 heat flow measurements were made in approximately 97 hours of bottom time. The 97 hours does not include ship transit time or instrument transit time through the water column, generally about 6 hours per station.

## **Background**

In young oceanic lithosphere, advective heat loss due to crustal hydrothermal circulation is superimposed on the slow conductive heat loss of the lithosphere (e.g., *Parsons and Sclater, 1977*). This advective heat loss through young oceanic crust drives the entire volume of the global ocean through the oceanic crust every few hundred thousand years (*Parsons and Sclater, 1977; Mottl and Wheat, 1994; Johnson and Pruis, 2003*). The resulting mass and energy flux influences the chemistry of the crust and ocean (e.g., *Mottl and Wheat, 1994*), is responsible for physical changes to the oceanic crust (e.g. *Carlson, 2011*), and helps support a global crustal biosphere (e.g., *Edwards et al., 2012*). Fluid flow is believed focused in the uppermost tens to

hundreds of meters of the upper oceanic crust based on observations of permeability (*Becker, 1996; Fisher, 1998; Becker and Fisher, 2000; Fisher, 2005*) and low temperature crustal alteration (e.g., *Alt et al., 1986a, 2010; Gillis and Robinson, 1990*).

Ridge flank hydrothermal circulation studies show that basement permeability, basement relief, and the thickness and extent of sediment cover strongly influence the vigor and pattern of fluid flow and the magnitude of advective heat loss (*Sclater et al., 1974, 1976; Anderson and Hobart, 1976; Davis et al., 1999*). Hydrothermal circulation dominates heat transfer where crustal permeabilities are high, temperature gradients and basement relief are sufficient to drive fluid flow, and there are regions of basement exposure for seawater to freely enter and exit the oceanic crust. In young seafloor near the ridge crest conditions are ideal for the upper oceanic crust to host vigorous ventilated hydrothermal convection. As crustal age increases, temperature gradients and crustal permeability decrease, and low permeability sediment accumulation isolates the high permeability crust from seawater. This age progression acts in concert to diminish heat loss by fluid flow.

Two diagnostic characteristics of advective heat loss through ridge flanks include heat flow values substantially lower on average than predicted by conductive thermal models of lithospheric evolution and significantly more variability than observations on older seafloor. In areas of hydrothermal circulation, heat flow values in sediment ponds are typically lower than expected heat flow due to the cooling effect of ventilation through surrounding basement exposures. Heat that would normally reach the surface in the absence of fluid flow is carried laterally through the underlying oceanic crust to a discharge region. This process lowers the thermal gradient in the overlying sediments that can be considerable distances from the exposed basement biasing heat flow observations towards lower values (e.g., *Baker et al., 1991; Fisher et al., 2003; Hutnak et al., 2008; Langseth et al., 1984, 1992*). This bias is made worse because measurements cannot be made in basement where discharge normally occurs. As a result, average heat flow is often well below predictions of conductive reference model. In areas of vigorous fluid flow where the sediment-crust interface is nearly isothermal, the thermal gradient is a strong function of sediment thickness giving rise to the increased variability in heat flow values (e.g., *Davis et al., 1989*).

## **Tectonic Setting and Previous Work**

All heat flow measurements were made on the southern flank of the Costa Rica Rift. This ridge flank has been the site of numerous seismic, heat flow and ocean drilling experiments and has become an important type location for investigations of off-axis hydrothermal processes (Anderson and Hobart, 1976; Langseth et al., 1983; Hobart et al., 1985). The spreading rate of 3.6-3.8 cm/yr (Hobart, 1985) gives rise to a relatively subdued abyssal hill basement relief of approximately 150 m (Swift et al., 1998; Bird and Pockalny, 1994). The sedimentation rate of 50 m/my (Sancetta, 1983) is relatively high due to its equatorial location.

On the southern flank of the Costa Rica Rift, previously collected heat flow measurements are not precisely navigated or collocated with seismic reflection data (Anderson and Hobart, 1976; Langseth et al., 1983; Hobart et al., 1985) making it difficult to evaluate the environmental context needed for an enhanced understanding hydrothermal circulation. Additionally the coarse spacing of early measurements makes them susceptible to aliasing. Nevertheless these coarse measurements show very low heat flow values near the ridge crest with values  $> 100 \text{ mW/m}^2$  below conductive predictions (Fisher et al., 1990). These low values characteristic of ‘ventilated’ oceanic crust transition to values consistent with plate cooling models over a distance of about 50 km in a region showing a significant increase in sediment thickness.

Newer measurements (Swift et al., 1998; Davis et al., 2003, 2004) overcome these issues but focused on ODP Holes 504A/B. These data show that shallow probe measurements are in good agreement with downhole heat flow (Davis et al., 2003), and that temperatures at the sediment-basement interface in the vicinity of ODP Holes 504A/B are between 50° and 70° C. Modeling indicates vigorous and warm fluid flow through layer 2 having an effective formation-scale permeability of  $10^{-9} \text{ m}^2$  (Davis et al., 2004). In spite of the high effective formation-scale permeability heat flow values are consistent with conductive reference models by about 5.1 Myr (~ 190 km from the ridge) (Fisher et al., 1990; Davis et al., 2004).

## Heat Flow Data

With the exception of heat flow station PB01 that is located within a sediment pond of the **Panama** fraction zone, heat flow stations were located along the eastern most north-south seismic line being collected during Expedition JC114 (**Figure 2**). Normally heat flow measurements should be collected after seismic reflection measurements but logistical

considerations made that timing impractical.

#### Heat flow station PB01

Heat flow station PB01 is located within a sediment pond of the **Panama** fracture zone. This station was used to test the heat flow instrumentation over a region where swath bathymetry and sub-bottom profiling data had been previously collected. The thinking was that if something had been wrong with the heat flow equipment there would time to fix it while swath bathymetry and sub-bottom profiling was run over the eastern most seismic line. Fortunately no problems were experienced during the collection of the data.

Heat flow station PB01 consists of 18 measurements that show a trend of increasing heat flow to the east that varies from about 140 to 190 mW m<sup>-2</sup> (**Figure 3**). The crustal age is approximately 5.5 my yielding a conductive prediction of 216 mW m<sup>-2</sup> and a fractional heat flow ( $q_{\text{obs}}/q_{\text{pred}}$ ) value of 0.74, where  $q_{\text{obs}}$  and  $q_{\text{pred}}$  are the observed and predicted heat flow.

#### Heat flow station PB02

Heat flow station PB02 is the northward most station and was positioned where sediment cover was thought to represent a minimum value to capture well ventilated hydrothermal circulation. This heat flow station consists of 19 measurements that covers two sediment ponds (**Figure 4**). The measurements have a nominal spacing of 200 m. In general the values are very low and relatively uniform with a mean and standard deviation of 41 and mW m<sup>-2</sup>, respectively. The crustal age in this area is 1.0 and the predicted conductive heat flow is 494 mW m<sup>-2</sup>, giving a fractional heat flow ( $q_{\text{obs}}/q_{\text{pred}}$ ) value of 0.08.

#### Heat flow station PB03

Heat flow station PB03 was positioned in a region of sparse sediment cover similar to station PB02. This heat flow station consists of 11 measurements over a region of generally increasing seafloor depth (**Figure 5**). Heat flow is more variable than station PB01 with a mean and standard deviation of 58 and 54 mW m<sup>-2</sup>, respectively. A single heat flow value of 216 mW m<sup>-2</sup>, located on a local bathymetric high, gives rise to the large standard deviation. The crustal age in this region is 2.3 my yielding a predicted conductive heat flow of 338 mW m<sup>-2</sup> and a fractional heat flow ( $q_{\text{obs}}/q_{\text{pred}}$ ) value of 0.17.

#### Heat flow station PB04

Heat flow station PB04 was positioned in a region of relatively more extensive but thin sediment cover. This heat flow station consists of 15 measurements with a nominal spacing of 400 to 600 m (**Figure 6**). Heat flow values vary between 6 and 322 mW m<sup>-2</sup> giving rise to a mean and standard deviation of 42 and 79 mW m<sup>-2</sup>, respectively. A single heat flow value of 322 mW m<sup>-2</sup>, located on a local bathymetric high, gives rise to the large standard deviation. The crustal age in this region is 2.3 my yielding a predicted conductive heat flow of 338 mW m<sup>-2</sup> and a fractional heat flow ( $q_{\text{obs}}/q_{\text{pred}}$ ) value of 0.17.

#### Heat flow station PB05

Heat flow station PB05 was positioned adjacent to previously collected data with the specific goal of assessing lateral variability (**Figure 7**). This station consists of 7 measurements with values ranging between 8 and 17 mW m<sup>-2</sup>. The mean and standard deviation are 14 and 7 mW m<sup>-2</sup>. The crustal age in this region is 4.2 my yielding a predicted conductive heat of 247 mW m<sup>-2</sup> and a fractional heat flow ( $q_{\text{obs}}/q_{\text{pred}}$ ) value of 0.06.

#### Heat flow station PB06

Heat flow station PB06 is the southern most station (**Figure 8**) along the eastern seismic line and is in the region with the greatest sediment thickness. This station consists of 15 measurements with values ranging between 90 and 896 mW m<sup>-2</sup>. The mean and standard deviation are 235 and 205 mW m<sup>-2</sup>, respectively. The crustal age in this region is 5.5 my and the predicted conductive heat flow is 216 mW m<sup>-2</sup> yielding a fractional heat flow value of 1.09. Although the mean and conductive heat flow are in agreement the significant variability indicates the presence of significant fluid flow.

### Discussion

Although additional analysis of these new heat flow data will await the collection of seismic data, **Figure 9**, places the new heat flow data within a regional context. In the absence of hydrothermal circulation the red line shows the predicted magnitude and distribution of heat flux at the seafloor. Hydrothermal circulation can redistribute and focus this heat flux as indicated by

the discrepancy between the data and model prediction. Low heat flow values near the ridge crest show the effect of ventilated hydrothermal circulation (e.g., heat flow stations PB01 – PB04). Sediment cover appears sparse and flow is unrestricted. The difference between the data and the station average provide estimates on the advective component of heat loss through the seafloor. Isolated heat flow highs may reflect areas of thin sediment cover or areas near exposed basement where fluids are actively discharging into the ocean. Starting near 150 km sediment thickness appears to increase and changes the style of hydrothermal circulation. Areas of exposed basement hosting discharge become more restricted and the basement warms. Complete basement burial isolates hydrothermal circulation to the upper crust.



## References

- Alt, J. C., J. Honnorez, C. Laverne, R. Emmermann, (1986) Hydrothermal alteration of a 1 km section through the upper oceanic crust, Deep Sea Drilling Project Hole 504B: mineralogy, chemistry, and evolution of seawater – basalt interactions, *J. Geophys. Res.*, *91*, 10309–10335.
- Alt, J. C., D. A. H. Teagle, C. Laverne, D. A. Vanko, W. Bach, J. Honnorez, K. Becker, M. Ayadi, P. A. Pezard (1996), Ridge-flank alteration of upper oceanic crust in the Eastern Pacific: synthesis of results for volcanic rocks of Holes 504B and 896A, *Proc. Ocean Drill. Prog., Sci. Results 148*, 435–450.
- Alt, J. C., C. Laverne, R. M. Coggon, D. A. H. Teagle, N. R. Banerjee, S. Morgan, C. E. Smith-Duque, M. Harris, and L. Galli (2010), Subsurface structure of a submarine hydrothermal system in ocean crust formed at the East Pacific Rise, ODP/IODP Site 1256, *Geochem. Geophys. Geosyst.*, *11*, Q10010, doi:10.1029/2010GC003144
- Anderson, R. N., and M. Hobart (1976), The relation between heat flow, sediment thickness, and age in the eastern Pacific, *J. Geophys. Res.*, *81*, 2968-2989.
- Anderson, R. N., J. Honnorez, K. Becker, A. C. Adamson, J. C. Alt, R. Emmermann, P. D. Kempton, H. Kinoshita, C. Laverne, M.J. Mottl, and R.L. Newmark (1982), DSDP Hole 504B, the first reference section over 1 km through Layer 2 of the oceanic crust, *Nature* *300* (1982) 589– 594.
- Baker, P. A., P. M. Stout, M. Kastner, and H. Elderfield (1991), Large-scale lateral advection of seawater through oceanic crust in the central equatorial Pacific, *Earth Planet. Sci. Lett.*, *105*, 522–533.
- Bird, R. T., and R. A. Pockalny (1994) Cretaceous and Cenozoic seafloor and oceanic basement roughness: Spreading rate, crustal age and sediment thickness correlations, *Earth Planet. Sci. Lett.*, *123*, 239-254.
- Becker, K. (1996), Permeability measurements in Hole 896A and implications for the lateral variability of upper crustal permeability at Sites 504 and 896, *Proc. Ocean Drill. Prog., Sci. Results 148*, 353– 363.
- Becker, K., and A.T. Fisher (2000), Permeability of upper oceanic basement on the eastern flank of the Juan de Fuca Ridge determined with drill-string packer experiments, *J. Geophys. Res.* *105*, 897– 912.

- K. Becker, H. Sakai, A. C. Adamson, J. Alexandrovich, J. C. Alt, R. N. Anderson, D. Bideau, R. Gable, P. M. Herzig, S. Houghton, H. Ishizuka, H. Kawahata, H. Kinoshita, M. G. Langseth, M. A. Lovell, J. Malpas, H. Masuda, R. B. Merrill, R. H. Morin, M. J. Mottl, J. E. Pariso, P. Pezard, J. Phillips, J. Sparks, and S. Uhlig, (1989), Drilling deep into young oceanic crust at Hole 504B, Costa Rica Rift, *Rev. Geophys.* 27, 79–102.
- Carlson, R. L. (2011), The effect of hydrothermal alteration on the seismic structure of the upper oceanic crust: Evidence from Holes 1256D and 504B, *Geochem. Geophys. Geosyst.*, 12, Q09013, doi:10.1029/2011GC003624.
- Davis, E. E., D. S. Chapman, K. Wang, H. Villinger, A. T. Fisher, S. W. Robinson, J. Grigel, D. Pribnow, J. Stein, and K. Becker (1999), Regional heat flow variations across the sedimented Juan de Fuca Ridge eastern flank: Constraints on lithospheric, *J. Geophys. Res.*, 104, 17,675–17,688.
- Davis, E.E., et al. (1989), Heat-flow variations correlated with buried basement topography on the Juan de Fuca Ridge flank, *Nature*, 342, 533-537.
- Davis, E. E., K. Becker, and J. He (2004), Costa Rica Rift revisited: Constraints on shallow and deep hydrothermal circulation in young oceanic crust, *Earth Planet. Sci. Lett.*, 222, 863–879.
- Detrick, R., J. Collins, R. Stephen, S. Swift, (1994) In situ evidence for the nature of the seismic layer 2/3 boundary in oceanic crust, *Nature* 370, 288– 290.
- Edwards, K.J., A.T. Fisher, and C.G. Wheat (2012), The deep subsurface biosphere in igneous ocean crust: frontier habitats for microbiological exploration, *Frontiers in microbiology*, 3
- Emile-Geay, J. and G. Madec (2009), Geothermal heating, diapycnal mixing and the abyssal circulation, *Ocean Sciences*, 5, 203-217.
- Fisher, A. T. (1998), Permeability within basaltic oceanic crust, *Rev. Geophys.*, 36, 143-182.
- Fisher, A. T., and K. Becker (1995), Correlation between seafloor heat flow and basement relief: Observational and numerical examples and implications for upper crustal permeability, *J. Geophys. Res.*, 100, 12,641–12,657.
- Fisher, A. T., K. Becker, I. T. N. Narasimhan, M. G. Langseth, and M. J. Mottl (1990), Passive, off-axis convection through the southern flank of the Costa Rica Rift, *J. Geophys. Res.*, 95, 9343–9370.
- Fisher, A. T., and C. G. Wheat (2010), Seamounts as conduits for massive fluid, heat, and solute fluxes on ridge flanks, *Oceanography*, 23, 74-87.

- Fisher, A.T., et al (2003a), Hydrothermal recharge and discharge across 50 km guided by seamounts on a young ridge flank, *Nature*, 421, 618-621.
- Fisher, A. T., C. A. Stein, R. N. Harris, K. Wang, E. A. Silver, M. Pfender, M. Hutnak, A. Cherkaoui, R. Bodzin, and H. Villinger (2003b), Abrupt thermal transition reveals hydrothermal boundary and role of seamounts within the Cocos Plate, *Geophys. Res. Lett.*, 30, doi:10.1029/2002GL016766.
- Gillis, K. M., and P. T. Robinson (1990), Patterns and processes of alteration in the lavas and dykes of the Troodos Ophiolite, Cyprus, *J. Geophys. Res.*, 95, 21,523–21,548.
- Hobart, M., M. Langseth, and R. Anderson (1985), *A geothermal and geophysical survey on the south flank of the Costa Rica Rift: Sites 504 and 505*. Anderson, RN, Honnorez, J., Becker, K., et al., *Init. Repts. DSDP*, 83, p. 379-404.
- Hofmann, M. and M.A. Morales Maqueda (2009), Geothermal heat flux and its influence on oceanic abyssal circulation and radiocarbon distribution, *Geophys. Res. Lett.*, 36, L03603, doi:10.1029/2008GL036078
- Hutnak, M., A. T. Fisher, R. Harris, C. Stein, K. Wang, G. Spinelli, M. Schindler, H. Villinger, and E. Silver (2008), Large heat and fluid fluxes driven through mid-plate outcrops on ocean crust, *Nature Geosci.*, 1, 611-614.
- Johnson, H. P., and M. J. Pruis (2003), Fluxes of fluid and heat from the oceanic crustal reservoir, *Earth Planet. Sci. Lett.*, 216, 565–574.
- Langseth, M. G., R. D. Hyndman, K. Becker, S. H. Hickman, and M. H. Salisbury (1984), The hydrogeological regime of isolated sediment ponds in mid-oceanic ridges, *Initial Rep. Deep Sea Drill. Proj.*, 78B, 825–837.
- Langseth, M. G., K. Becker, R. P. Von Herzen, and P. Schultheiss (1992), Heat and fluid flux through sediment on the western flank of the Mid-Atlantic Ridge: A hydrogeological study of North Pond, *Geophys. Res. Lett.*, 19, 517–520.
- Mottl, M. J., and C. G. Wheat (1994), Hydrothermal circulation through mid-ocean ridge flanks: Fluxes of heat and magnesium, *Geochim. Cosmochim. Acta*, 58, 2225–2237.
- Parsons, B., and J. Sclater (1977), An analysis of the variation of ocean floor bathymetry and heat flow with age, *J. Geophys. Res.*, 82, 803–827.
- S.A. Swift, G.M. Kent, R.S. Detrick, J.A. Collins, R.A. (1998), Stephen, Oceanic basement structure, sediment thickness, and heat flow near Hole 504B, *J. Geophys. Res.* 103, 15377–

15391.

Sancetta, C .A., (1983), Biostratigraphic and paleoceanographic events in the eastern equatorial Pacific, *Initial Rep. Deep Sea Drill. Proj.*, 69, 311-319.

Sclater, J., R. P. Von Herzen, D. L. Williams, R. N. Anderson, and K. Klitgord (1974), The Galapagos Spreading Centre: Heat flow low on the North Flank, *Geophys. J. Roy. Astr. Soc.*, 38, 609-626.

Sclater, J.G., J. Crowe, and R.N. Anderson (1976), On the reliability of oceanic heat flow averages, *J. Geophys. Res.*, 81, 2997-3006.

S.A. Swift, G.M. Kent, R.S. Detrick, J.A. Collins, R.A. Stephen (1998), Oceanic basement structure, sediment thickness, and heat flow near Hole 504B, *J. Geophys. Res.* 103, 15,377–15,391.

Table 1. Multipenetration heat flow data

Station- Penetration	Date	Time	Latitude		Longitude		Thermal Grad.	Thermal Cond.	Heat Flow	Tilt	Depth
		(GMT)	(Deg)	(min)	(Deg)	(min)	(C/km)	(W/m/K)	(mW/m <sup>2</sup> )	(Deg)	(m)
PB01-01	14-Dec-14	16:24	1	14.0040	-84	37.0500	193	0.7	142	0.5	3447
PB01-02	14-Dec-14	17:35	1	14.0040	-84	36.9360	193	0.7	140	0.4	3450
PB01-03	14-Dec-14	18:36	1	14.0100	-84	36.8340	196	0.7	138	0.1	3451
PB01-04	14-Dec-14	19:42	1	14.0160	-84	36.7260	191	0.8	144	0.5	3454
PB01-05	14-Dec-14	20:52	1	14.0160	-84	36.5040	188	0.8	144	0.5	3459
PB01-06	14-Dec-14	22:02	1	14.0280	-84	36.2880	196	0.7	144	0.2	3472
PB01-07	14-Dec-14	23:09	1	14.0280	-84	36.0660	231	0.7	163	0.3	3481
PB01-08	15-Dec-14	0:17	1	14.0280	-84	35.8560	214	0.7	154	0.1	3487
PB01-09	15-Dec-14	1:25	1	14.0280	-84	35.6460	217	0.7	157	0.4	3498
PB01-10	15-Dec-14	2:39	1	14.0280	-84	35.4300	224	0.8	170	0.5	3504
PB01-11	15-Dec-14	3:45	1	14.0280	-84	35.2080	226	0.7	161	1.1	3507
PB01-12	15-Dec-14	4:54	1	14.0280	-84	34.9980	253	0.7	174	1.9	3511
PB01-13	15-Dec-14	6:07	1	14.0400	-84	34.7760	247	0.7	171	0.9	3524
PB01-14	15-Dec-14	7:14	1	14.0400	-84	34.5780	235	0.7	166	1.1	3557
PB01-15	15-Dec-14	8:30	1	14.0460	-84	34.3500	242	0.7	170	1.7	3552
PB01-16	15-Dec-14	9:40	1	14.0460	-84	34.1220	244	0.7	177	0.4	3568
PB01-17	15-Dec-14	10:50	1	14.0520	-84	33.9120	274	0.7	190	1.1	3574
PB01-18	15-Dec-14	11:21	1	14.0520	-84	33.9060	211	0.9	187	0.2	3562

Table 1. Multipenetration heat flow data - continued

Station-Penetration	Date	Time	Latitude		Longitude		Thermal Grad.	Thermal Cond.	Heat Flow	Tilt	Depth
		(GMT)	(Deg)	(min)	(Deg)	(min)	(C/km)	(W/m/K)	(mW/m2)	(Deg)	(m)
PB02-01	16-Dec-14	15:39	2	53.3820	-83	41.9460	62	0.7	45	2.9	3144
PB02-02	16-Dec-14	16:30	2	53.2680	-83	41.9520	51	0.7	37	3.3	3149
PB02-03	16-Dec-14	17:19	2	53.1660	-83	41.9580	52	0.7	37	3.5	3148
PB02-04	16-Dec-14	18:08	2	53.0580	-83	41.9580	55	0.7	40	3.1	3151
PB02-05	16-Dec-14	18:57	2	52.9500	-83	41.9580	59	0.7	42	3.3	3127
PB02-06	16-Dec-14	19:47	2	52.9500	-83	41.9640	48	0.7	35	3.3	3127
PB02-07	16-Dec-14	22:19	2	51.5760	-83	41.9880	48	0.7	35	2.9	3166
PB02-08	16-Dec-14	23:14	2	51.4680	-83	41.9940	45	0.7	32	2.9	3169
PB02-09	17-Dec-14	0:07	2	51.3600	-83	41.9940	45	0.7	33	2.8	3176
PB02-10	17-Dec-14	1:05	2	51.2520	-83	41.9940	46	0.7	33	2.9	3176
PB02-11	17-Dec-14	2:01	2	51.1440	-83	42.0000	47	0.7	34	2.9	3194
PB02-12	17-Dec-14	2:45	2	51.0900	-83	42.0060	48	0.7	35	2.6	3215
PB02-13	17-Dec-14	3:10	2	50.9820	-83	42.0060	73	0.7	52	2.8	3235
PB02-14	17-Dec-14	4:30	2	50.8740	-83	42.0120	62	0.7	45	2.6	3167
PB02-15	17-Dec-14	5:26	2	50.7120	-83	42.0180	60	0.7	44	3.3	3149
PB02-16	17-Dec-14	6:19	2	50.5980	-83	42.0180	65	0.7	47	2.9	3145
PB02-17	17-Dec-14	7:13	2	50.4960	-83	42.0240	97	0.7	72	2.4	3161
PB02-18	17-Dec-14	9:18	2	49.7940	-83	42.0480	61	0.7	44	3.1	3193
PB02-19	17-Dec-14	10:34	2	49.5780	-83	42.0480	52	0.7	37	3.0	3234

Station-Penetration	Date	Time	Latitude		Longitude		Thermal Grad.	Thermal Cond.	Heat Flow	Tilt	Depth
		(GMT)	(Deg)	(min)	(Deg)	(min)	(C/km)	(W/m/K)	(mW/m2)	(Deg)	(m)
PB03-01	17-Dec-14	22:12	2	34.2660	-83	42.4440	46	0.7	34	2.8	3144
PB03-02	17-Dec-14	23:12	2	33.9420	-83	42.4500	61	0.7	44	3.1	3140
PB03-03	18-Dec-14	0:50	2	33.6240	-83	42.4560	53	0.7	37	2.4	3191
PB03-04	18-Dec-14	2:10	2	33.2940	-83	42.4680	53	0.7	38	1.8	3187
PB03-05	18-Dec-14	3:27	2	32.9700	-83	42.4740	65	0.7	46	2.6	3223
PB03-06	18-Dec-14	4:43	2	32.6400	-83	42.4800	58	0.7	41	3.0	3275
PB03-07	18-Dec-14	6:04	2	32.3160	-83	42.4980	278	0.8	216	2.8	3248
PB03-08	18-Dec-14	8:30	2	31.3440	-83	42.5220	55	0.7	40	2.8	3288
PB03-09	18-Dec-14	9:57	2	31.0260	-83	42.5340	48	0.7	34	3.7	3315
PB03-10	18-Dec-14	11:16	2	30.7020	-83	42.5400	44	0.7	31	3.1	3332
PB03-11	18-Dec-14	12:38	2	30.3840	-83	42.5460	103	0.7	73	3.1	3345

Table 1. Multipenetration heat flow data - continued

Station- Penetration	Date	Time	Latitude		Longitude		Thermal Grad.	Thermal Cond.	Heat Flow	Tilt	Depth
		(GMT)	(Deg)	(min)	(Deg)	(min)	(C/km)	(W/m/K)	(mW/m2)	(Deg)	(m)
PB04-01	19-Dec-14	2:45	2	18.6300	-83	42.7440	9	0.7	6	2.3	3144
PB04-02	19-Dec-14	3:56	2	18.4140	-83	42.7500	9	0.7	6	3.2	3149
PB04-03	19-Dec-14	5:07	2	18.1980	-83	42.7560	8	0.8	6	3.1	3148
PB04-04	19-Dec-14	6:21	2	17.9820	-83	42.7560	11	0.7	8	3.3	3151
PB04-05	19-Dec-14	7:32	2	17.7600	-83	42.7560	44	0.7	31	4.0	3127
PB04-06	19-Dec-14	8:44	2	17.5500	-83	42.7620	18	0.7	12	3.1	3127
PB04-07	19-Dec-14	9:50	2	17.3280	-83	42.7620	12	0.7	8	3.1	3166
PB04-08	19-Dec-14	11:01	2	17.0760	-83	42.7620	19	0.7	13	3.5	3169
PB04-09	19-Dec-14	12:22	2	16.7520	-83	42.7560	71	0.7	50	3.5	3176
PB04-10	19-Dec-14	14:42	2	15.7800	-83	42.7500	43	0.7	31	3.0	3176
PB04-11	19-Dec-14	16:04	2	15.4560	-83	42.7440	44	0.7	30	2.4	3194
PB04-12	19-Dec-14	17:24	2	15.1320	-83	42.7560	29	0.7	20	3.0	3215
PB04-13	19-Dec-14	18:50	2	14.8260	-83	42.7560	437	0.7	322	2.9	3235
PB04-14	19-Dec-14	20:17	2	14.4780	-83	42.7560	34	0.7	24	3.5	3167
PB04-15	19-Dec-14	21:38	2	14.1540	-83	42.7560	83	0.7	60	2.5	3149

Station- Penetration	Date	Time	Latitude		Longitude		Thermal Grad.	Thermal Cond.	Heat Flow	Tilt	Depth
		(GMT)	(Deg)	(min)	(Deg)	(min)	(C/km)	(W/m/K)	(mW/m2)	(Deg)	(m)
PB05-01	20-Dec-14	12:21	2	0.2280	-83	43.1220	19	0.7	14	2.3	3144
PB05-02	20-Dec-14	13:28	2	0.0180	-83	43.1280	23	0.7	17	3.0	3140
PB05-03	20-Dec-14	14:40	1	59.7960	-83	43.1340	12	0.7	8	3.1	3191
PB05-04	20-Dec-14	15:52	1	59.5860	-83	43.1460	17	0.7	12	3.6	3187
PB05-05	20-Dec-14	16:56	1	59.4180	-83	43.1160	42	0.7	30	3.2	3223
PB05-06	20-Dec-14	19:41	1	57.7200	-83	43.1640	14	0.7	10	3.0	3275
PB05-07	20-Dec-14	20:46	1	57.5100	-83	43.1820	5	2.0	10	5.0	3248

Table 1. Multipenetration heat flow data - continued

Station- Penetration	Date	Time	Latitude	Longitude	Thermal Grad.	Thermal Cond.	Heat Flow	Tilt	Depth		
		(GMT)	(Deg)	(min)	(Deg)	(min)	(C/km)	(W/m/K)	(mW/m2)	(Deg)	(m)
PB06-01	21-Dec-14	2:06	1	38.7180	-83	44.4540	188	0.7	137	4.0	3482
PB06-02	21-Dec-14	3:22	1	38.5140	-83	44.4300	198	0.7	144	0.9	3538
PB06-03	21-Dec-14	4:38	1	38.3280	-83	44.4240	210	0.7	155	0.7	3541
PB06-04	21-Dec-14	6:01	1	38.0700	-83	44.3820	1157	0.8	896	0.9	3533
PB06-05	21-Dec-14	7:21	1	37.8540	-83	44.3580	397	0.8	301	0.4	3547
PB06-06	21-Dec-14	8:45	1	37.6380	-83	44.3460	259	0.7	190	0.6	3557
PB06-07	21-Dec-14	9:56	1	37.4340	-83	44.3280	161	0.7	118	1.2	3555
PB06-08	21-Dec-14	11:18	1	37.1580	-83	44.3280	229	0.7	165	1.7	3575
PB06-09	21-Dec-14	12:27	1	37.0020	-83	44.3220	382	0.7	276	1.7	3528
PB06-10	21-Dec-14	13:40	1	36.7860	-83	44.2860	418	0.7	305	1.4	3426
PB06-11	21-Dec-14	14:56	1	36.5700	-83	44.2620	570	0.7	411	2.0	3448
PB06-12	21-Dec-14	16:13	1	36.3600	-83	44.2380	190	0.7	135	1.3	3470
PB06-13	21-Dec-14	17:33	1	36.1440	-83	44.2080	130	0.7	94	0.9	3467
PB06-14	21-Dec-14	18:48	1	35.9220	-83	44.1900	125	0.7	90	1.6	3289
PB06-15	21-Dec-14	20:06	1	35.7060	-83	44.1660	156	0.7	111	0.9	3262



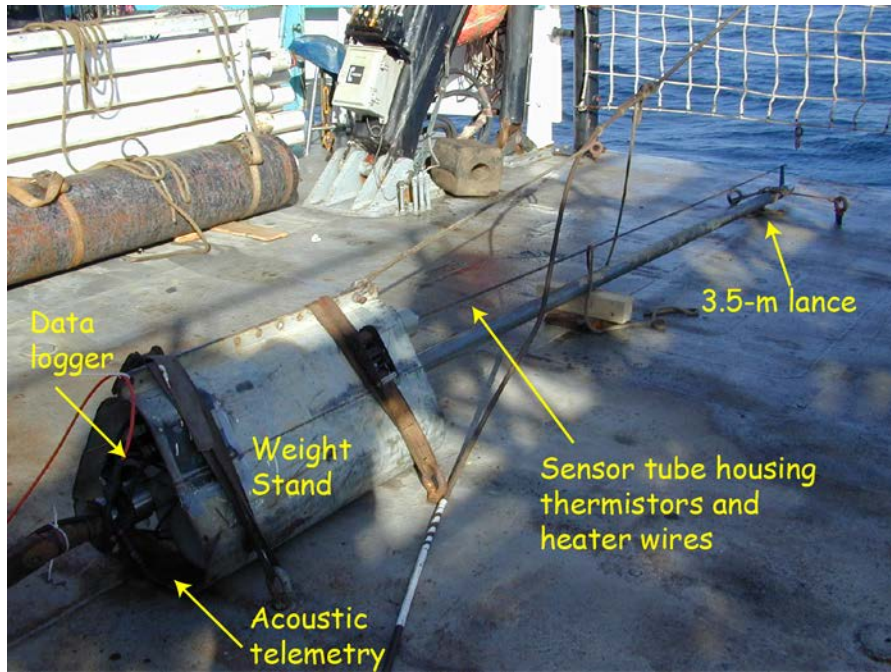


Figure 1. Multipenetration heat flow probe showing its various components.

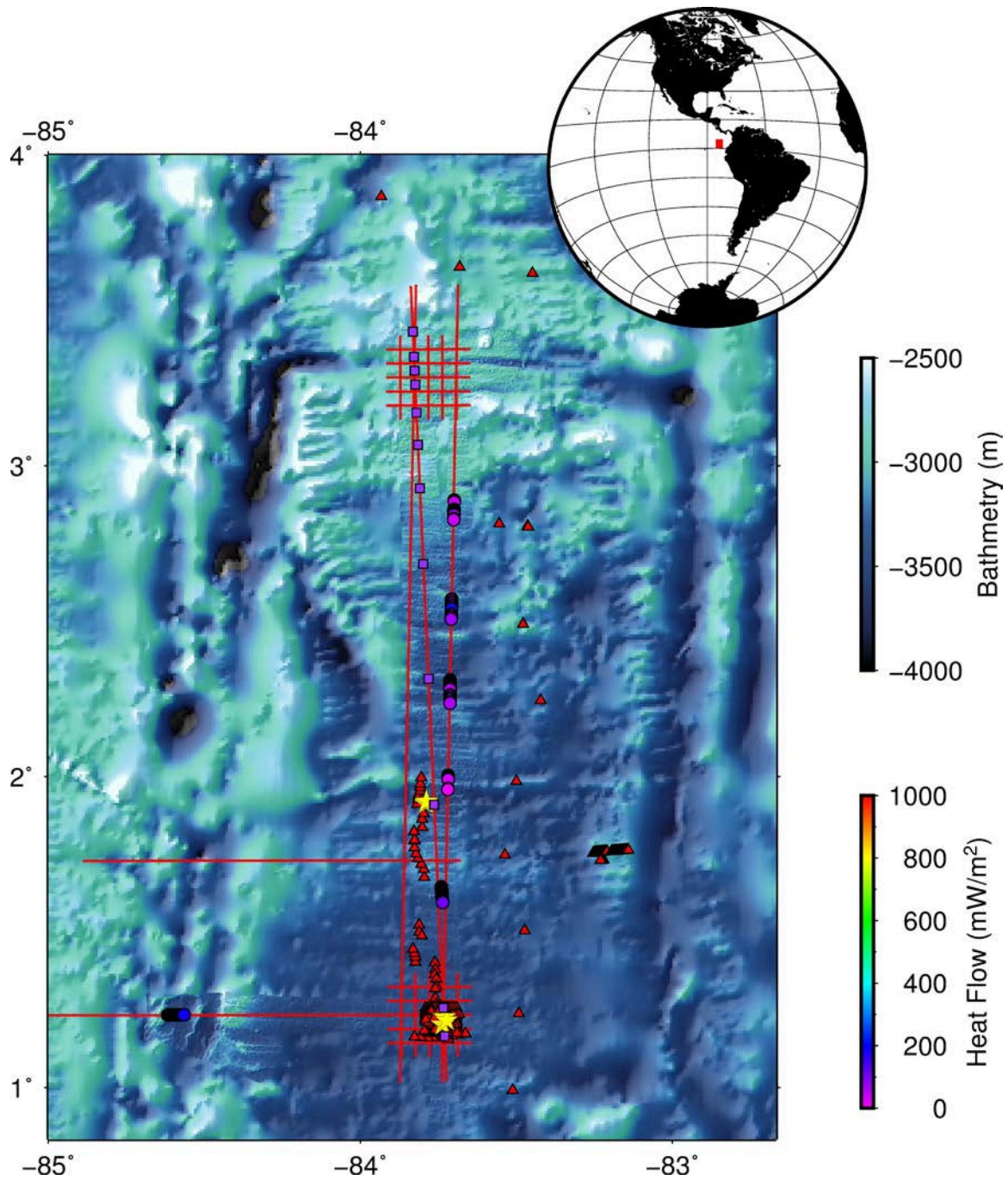


Figure 2. Southern flank of the Costa Rica rift showing pre-existing heat flow data (red triangles) and heat flow data collected on Expedition JC113. Purple squares show location of deployed magnetotelluric landers, red line show proposed seismic reflection profiles. Yellow stars show location of scientific boreholes. Red square on inset shows field area.

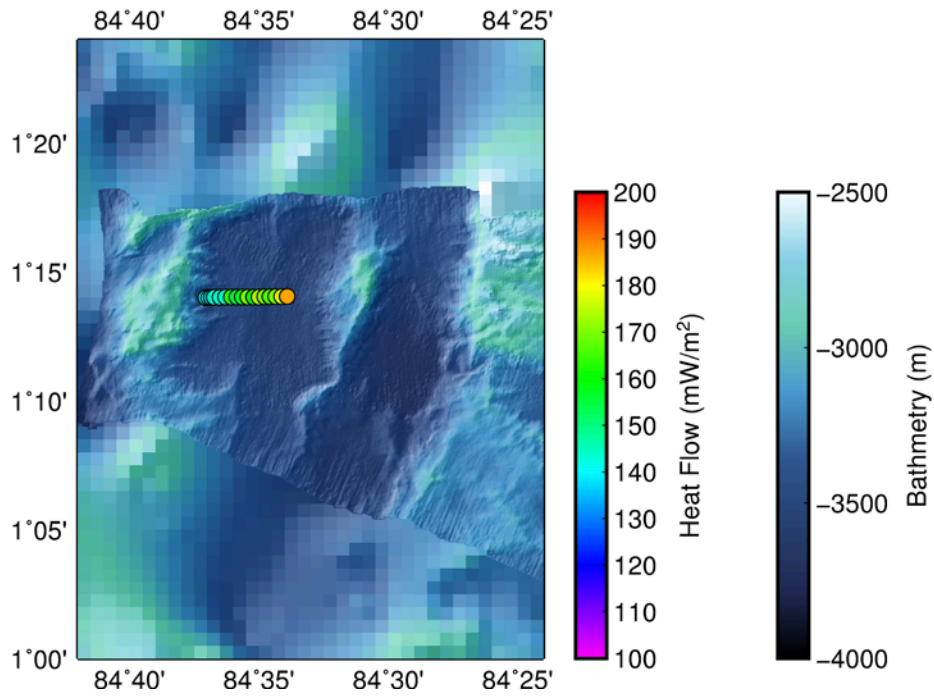
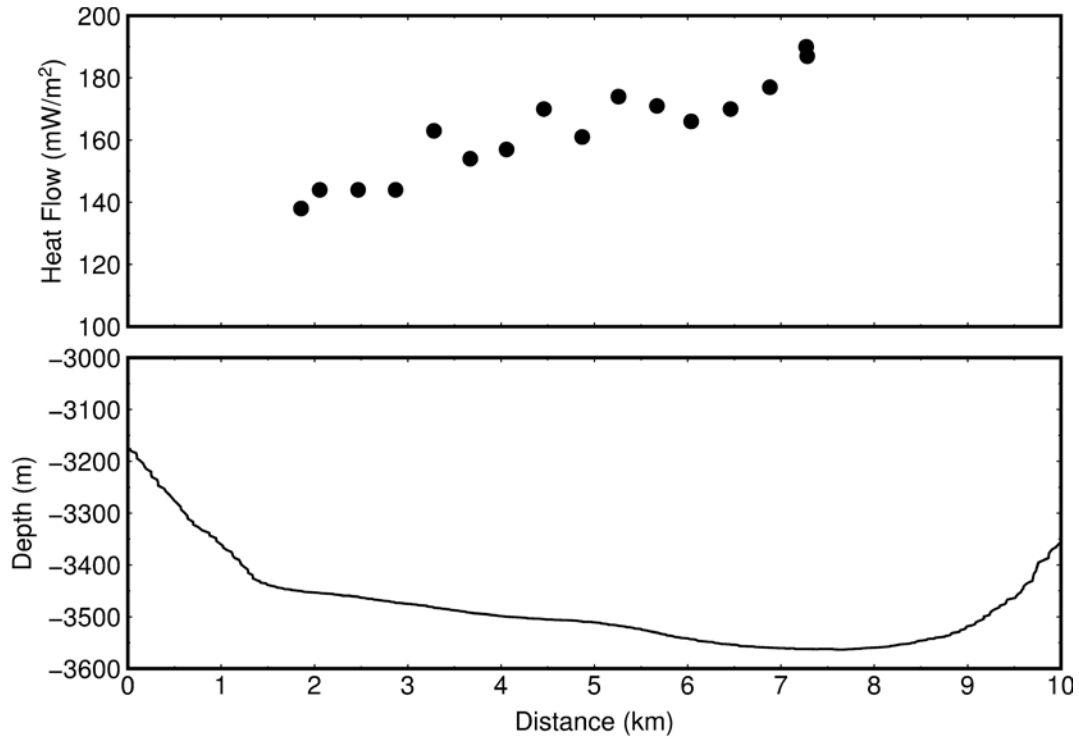


Figure 3. Heat flow station PB01 showing a) heat flow, b) bathymetry, c) location of heat flow data.

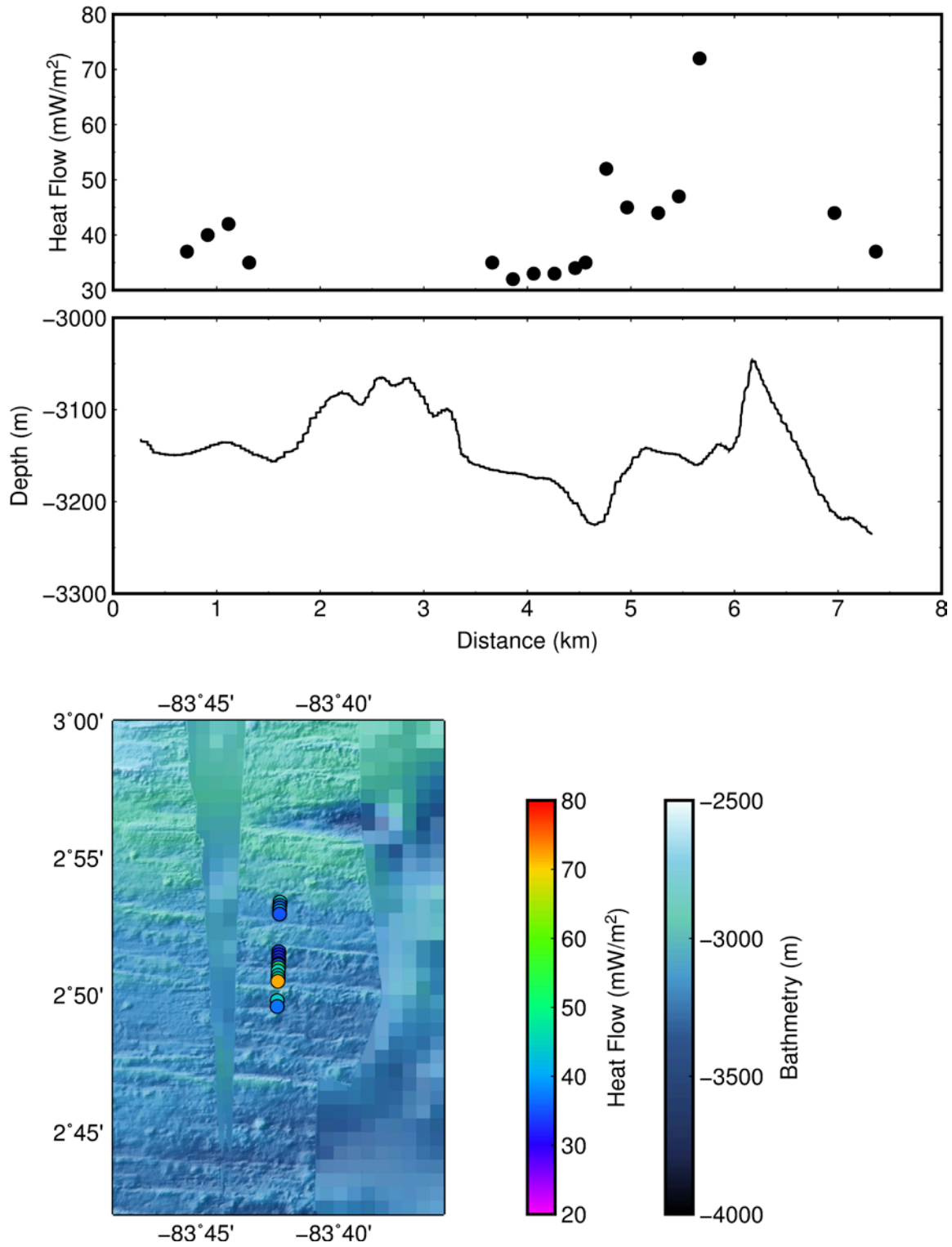


Figure 4. Heat flow station PB02 showing a) heat flow, b) bathymetry, c) location of heat flow data.

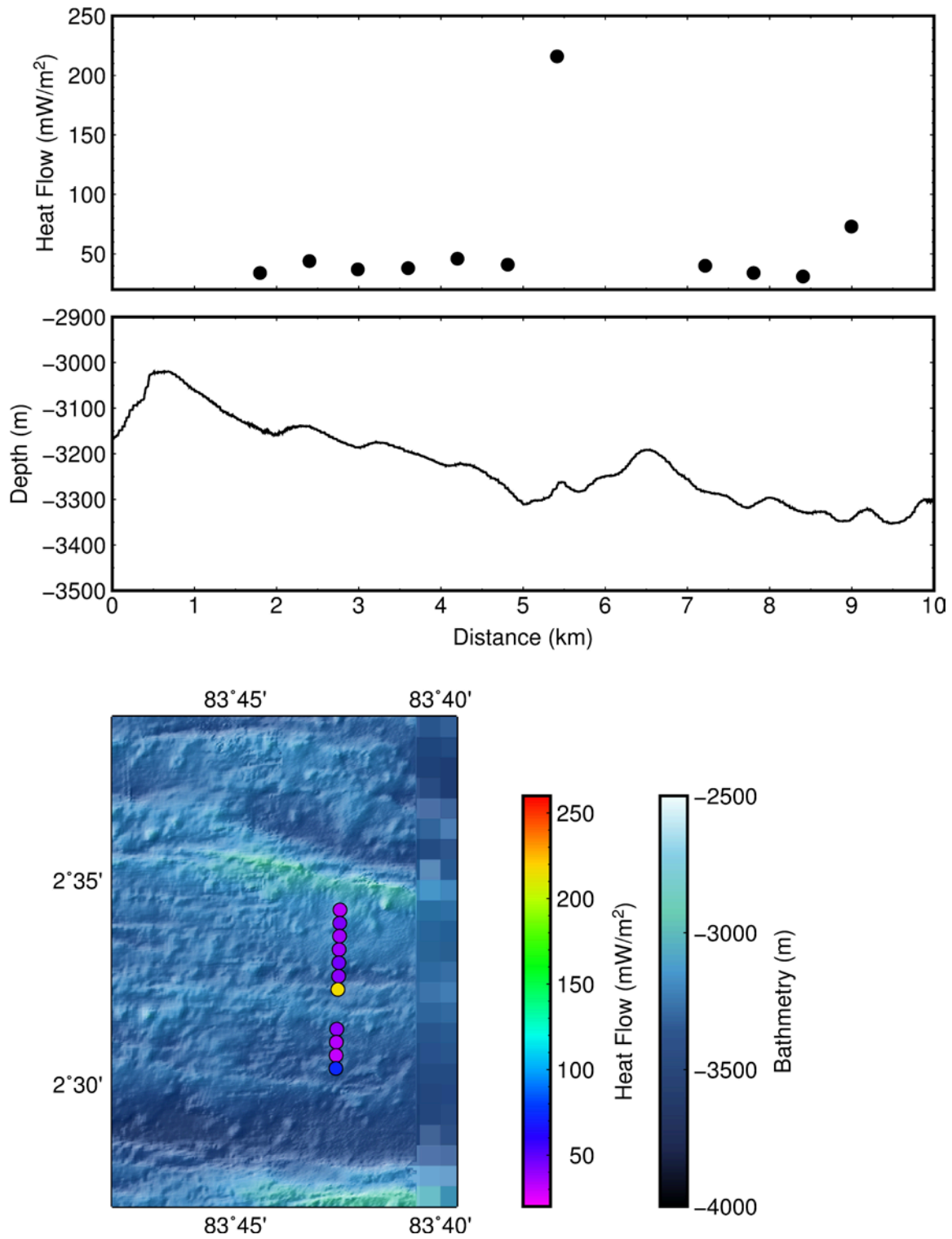


Figure 5. Heat flow station PB03 showing a) heat flow, b) bathymetry, c) location of heat flow data.

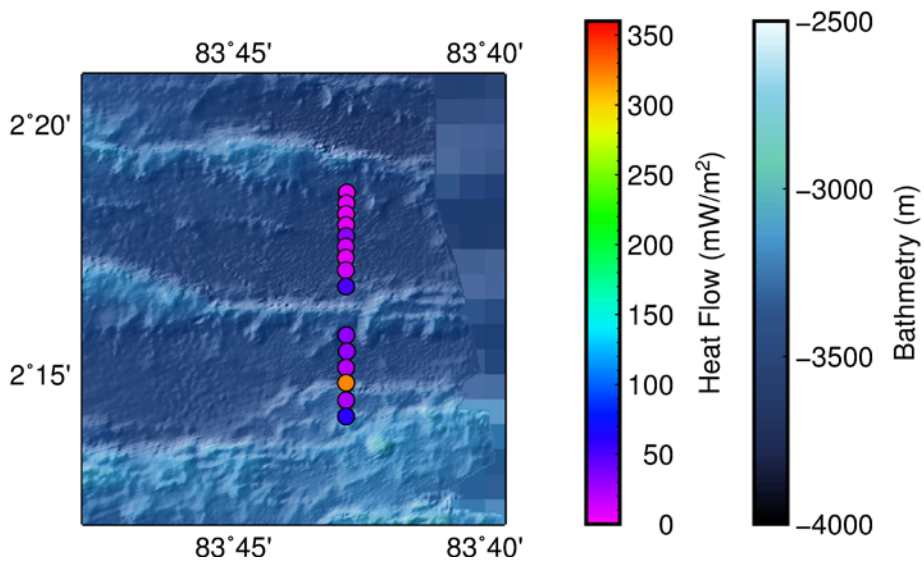
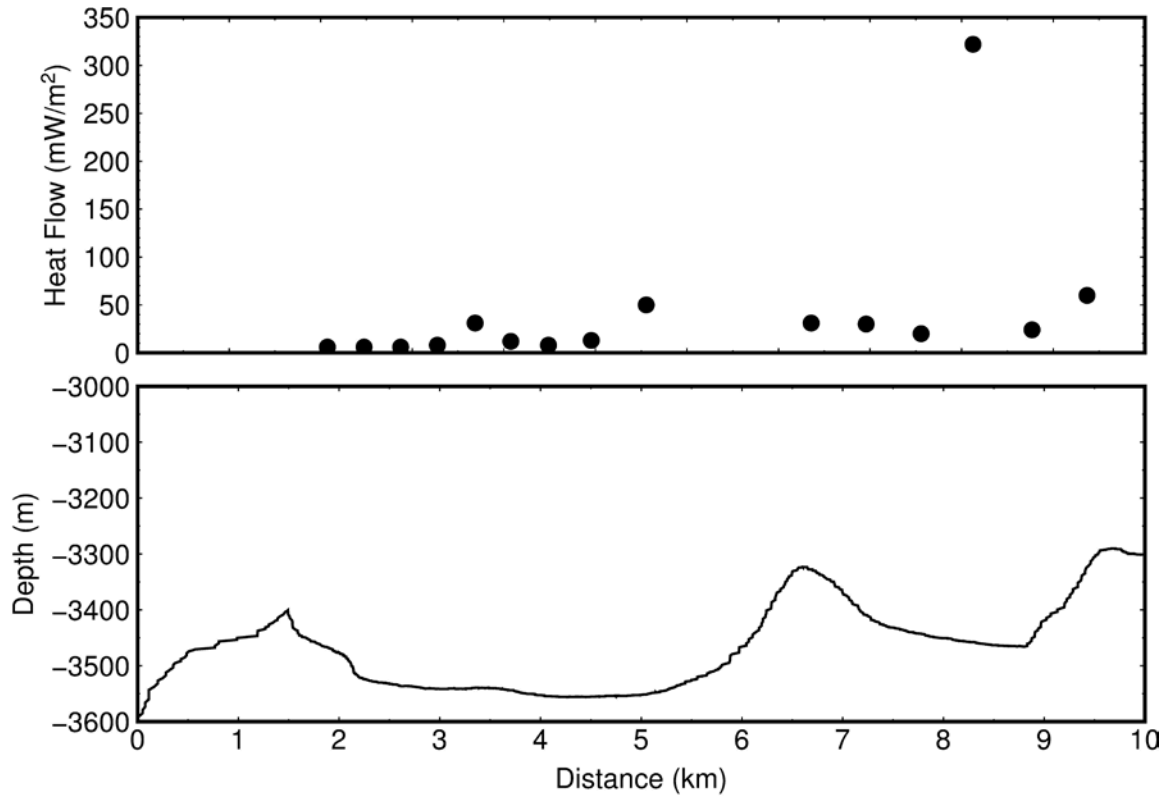


Figure 6. Heat flow station PB04 showing a) heat flow, b) bathymetry, c) location of heat flow data.

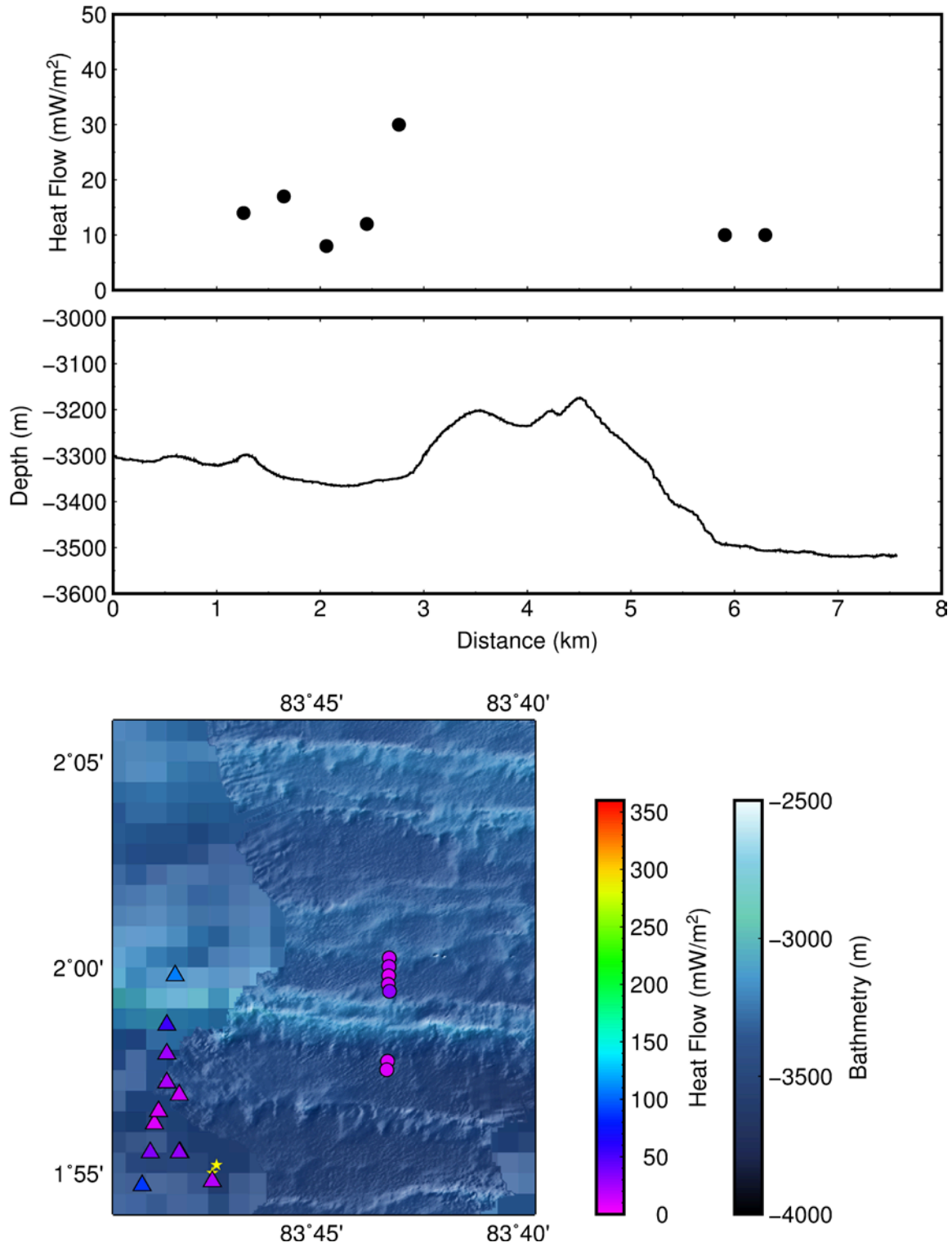


Figure 7. Heat flow station PB05 showing a) heat flow, b) bathymetry, c) location of heat flow data.

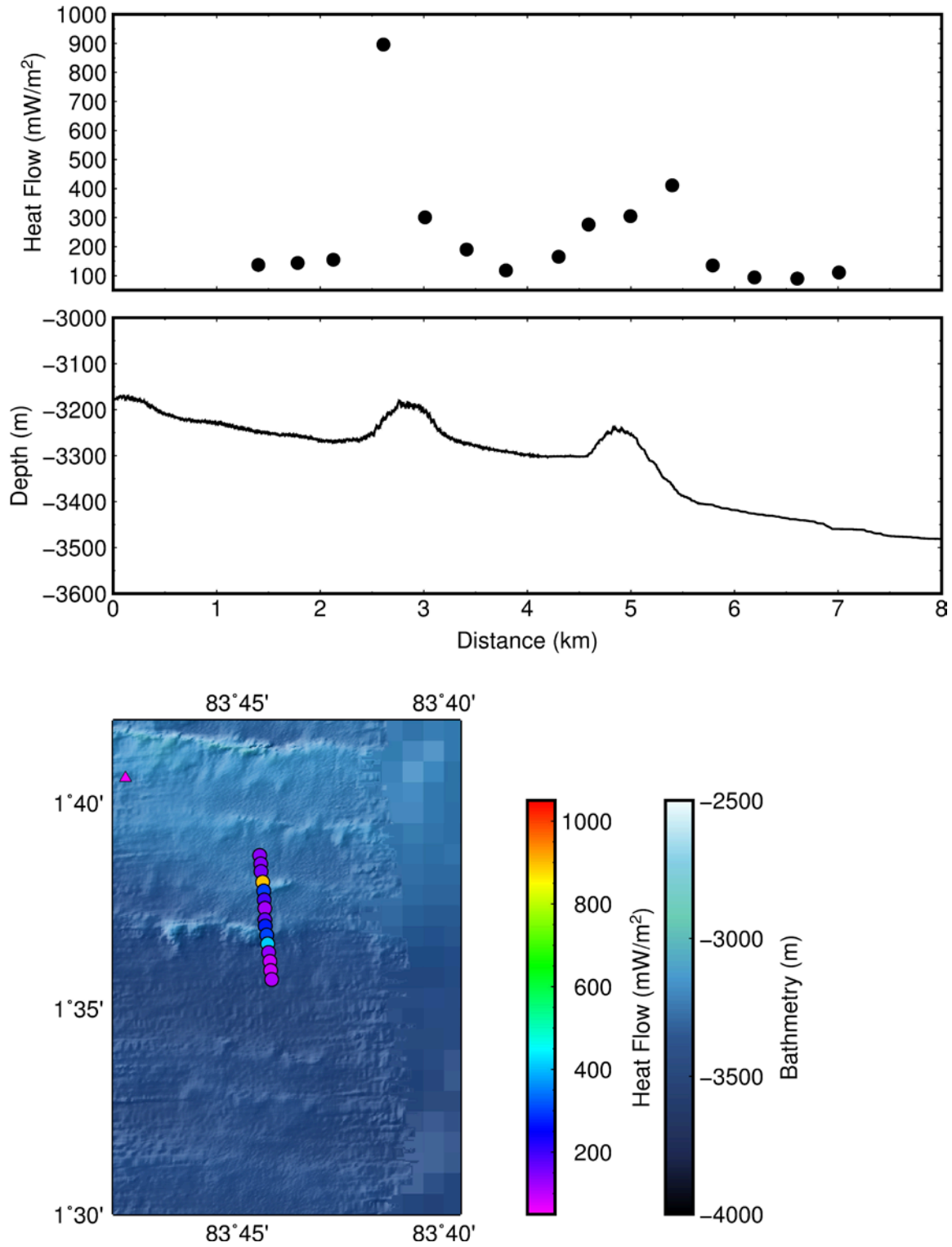


Figure 8. Heat flow station PB06 showing a) heat flow, b) bathymetry, c) location of heat flow data.



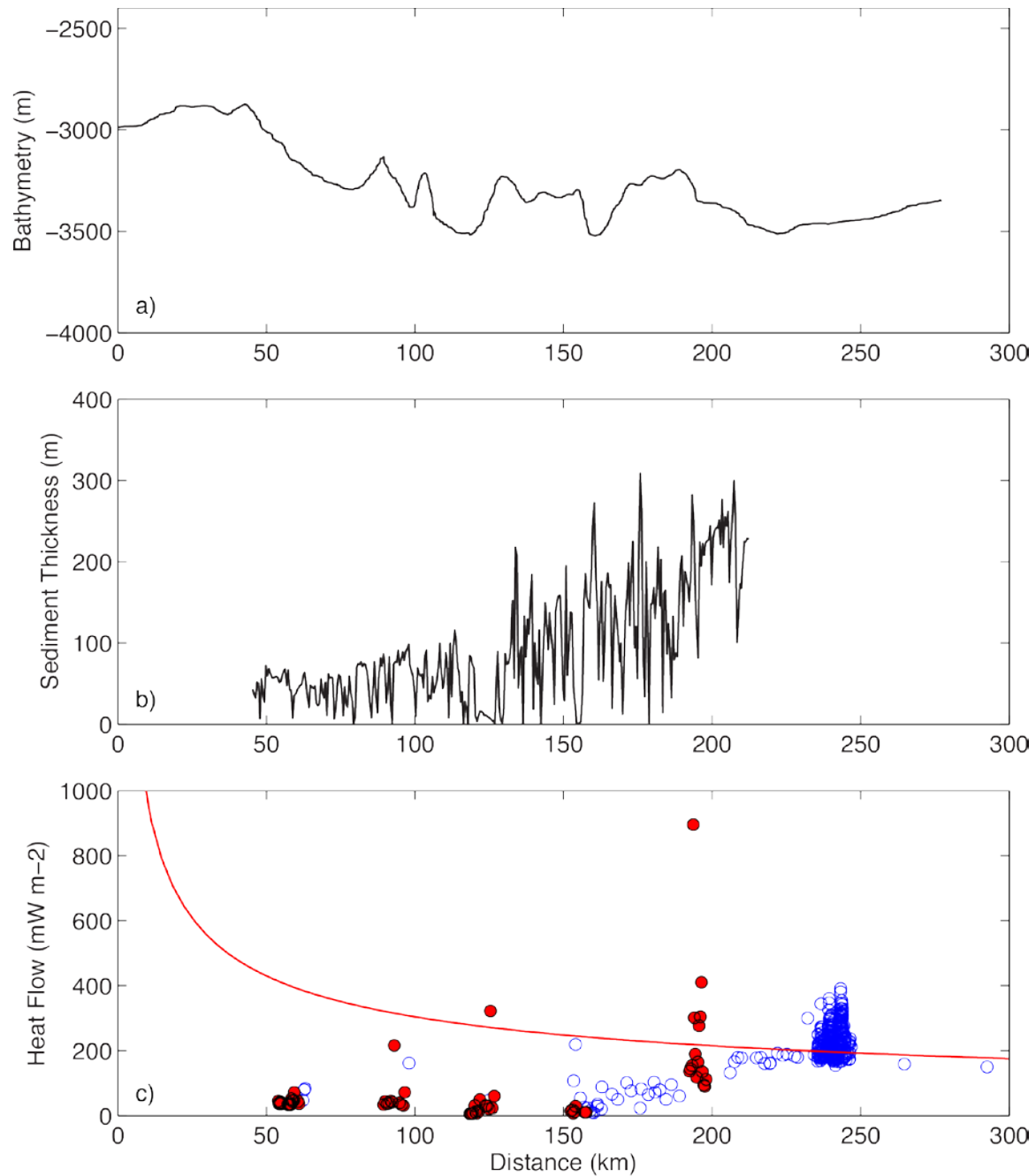


Figure 9. Thermal regime of the southern Costa Rica ridge flank. a) bathymetry, b) sediment thickness (Floyd et al., 2002, 2011), c) heat flow data. Open symbols show pre-existing data and closed red circles show data collected during expedition JC113. Red line shows predicted conductive heat flow.